

Article

Fabrication of Novel Cyanuric Acid Modified g-C₃N₄/Kaolinite Composite with Enhanced Visible Light-Driven Photocatalytic Activity

Zhiming Sun ^{1,*}, Fang Yuan ¹, Xue Li ¹, Chunquan Li ¹, Jie Xu ¹ and Bin Wang ^{2,*}¹ School of Chemical and Environmental Engineering, China University of Mining and Technology (Beijing), Beijing 100083, China; yfcumtb@163.com (F.Y.); lixuelucy@yeah.net (X.L.); lcqksy@163.com (C.L.); 13126852095@163.com (J.X.)² Beijing Key Laboratory of Clothing Materials R & D and Assessment, Beijing Engineering Research Center of Textile Nanofiber, School of Materials Science and Engineering, Beijing 100029, China

* Correspondence: zhimingsun@cumtb.edu.cn (Z.S.); 20150010@bift.edu.cn (B.W.); Tel.: +86-10-62339920 (Z.S.)

Received: 2 September 2018; Accepted: 1 October 2018; Published: 7 October 2018



Abstract: A novel kind of cyanuric-acid-modified graphitic carbon nitride (g-C₃N₄)/kaolinite (m-CN/KA) composite with enhanced visible light-driven photocatalytic performance was fabricated through a facile two-step process. Rhodamine B (RhB) was taken as the target pollutant to study the photocatalytic performance of the synthesized catalysts. It is indicated that the cyanuric acid modification significantly enhanced photocatalytic activity under visible light illumination in comparison with the other reference samples. The apparent rate constant of m-CN/KA is almost 1.9 times and 4.0 times those of g-C₃N₄/kaolinite and bare g-C₃N₄, respectively. The superior photocatalytic performance of m-CN/KA could be ascribed, not only to the generation of abundant pore structure and reactive sites, but also to the efficient separation of the photogenerated electron-hole pairs. Furthermore, the possible photocatalytic degradation mechanism of m-CN/KA was also presented in this paper. It could be anticipated that this novel and efficient, metal-free, mineral-based photocatalytic composite has great application prospects in organic pollutant degradation.

Keywords: kaolinite; photocatalysis; cyanuric acid modification; g-C₃N₄

1. Introduction

In the past few decades, the problem of industrial and domestic wastewater was becoming more and more serious. A great amount of wastewater was discharged directly due to its complicated and expensive treatment process, resulting in severe damage to soil and water resources. Accordingly, highly efficient removal and degradation of wastewater has attracted a great deal of attention from environmental scientific research in the past few years [1–3]. Several approaches have been proposed to resolve this problem, such as ultrafiltration [4], absorption [5], and biological treatment [6]. Nevertheless, these methods face many drawbacks like high-cost, low-efficiency, non-recyclable, etc. Hence, semiconductor-based photocatalysis, a highly efficient, non-toxic, and low-cost method, which can degrade a variety of pollutants in wastewater via a series of simple redox reactions under illumination should be one kind of promising technology in treating wastewater [7,8]. However, some conventional semiconductor photocatalysts like ZnO and TiO₂ in a pure form have less visible responses, which severely restrict their practical application [9]. Therefore, the fabrication of high-activity, visible light-driven photocatalysts have become a hot topic.

In recent years, graphitic carbon nitride ($\text{g-C}_3\text{N}_4$) has been widely researched in photocatalysis, owing to its superior visible-light response, stable structure, metal-free and environmentally friendly superiority, after being reported by Wang et al. [10,11]. Since Niu et al. [12] successfully developed covalent solid carbon nitride using laser sputtering technology, extensive research has investigated preparation methods of $\text{g-C}_3\text{N}_4$, such as HTHP (high temperature and high pressure) process [13], solid-phase synthesis [14], and liquid-phase electrodeposition [15]. Compared with the other methods, thermal polymerization is considered to be the most common method for synthesizing $\text{g-C}_3\text{N}_4$ because of it is easy-to-operate, low cost, there is an availability of raw materials, and has a better crystal form [16]. However, a photocatalyst prepared by the thermal polymerization method has the disadvantages of low specific surface area and low utilization of visible light. According to previous reports, if $\text{g-C}_3\text{N}_4$ could be completely exfoliated to monolayers, the specific surface area would increase several times [17]. In order to improve the photocatalytic properties of visible-light irradiation, many researchers have put great effort into modification using various methods, such as metallic elements doping, construction of semiconductor heterojunction, precious metal deposition, and organic acid modification. For instance, Wang et al. [18] successfully designed a K-modified $\text{g-C}_3\text{N}_4$ by facile thermal polymerization with KBr as the K source, where the rate of H_2 evolution was 5.6 times compared to pure $\text{g-C}_3\text{N}_4$. Sridharan et al. [19] synthesized $\text{g-C}_3\text{N}_4/\text{TiO}_2$ using thermal transformation methodology, resulting in better pollutant degradation due to a synergistic heterojunction between $\text{g-C}_3\text{N}_4$ and TiO_2 . Shalom et al. [20] reported a new and facile approach to form an ordered hollow carbon nitride structure, using a cyanuric acid-melamine (CM) complex in ethanol as the starting precursor. These methods are mainly used to restrain the recombination and prolong the life of photo-carriers in $\text{g-C}_3\text{N}_4$ by increasing the specific surface area of the catalyst, replacing the in-situ lattice, producing a Schottky barrier, generating an impurity level, and then improving photoactivity. Although these modification methods can partially improve the defects of $\text{g-C}_3\text{N}_4$, it is still hard to avoid the disadvantages of easy aggregation, difficult separation, high production cost, and low adsorption capacity [21].

Currently, a number of studies have paid close attention to composites based on natural minerals supporting catalyst nanoparticles due to their low-cost, non-toxic, high adsorption, and chemical stability [22,23]. It has been demonstrated that photocatalytic efficiency can be improved after the introduction of natural minerals, which can, not only retain the photocatalytic activity of the catalyst, but also promote rapid pollutant adsorption on the surface of the composite photocatalyst [24,25]. Among the various natural minerals carriers, kaolinite appears to be a superior candidate as a $\text{g-C}_3\text{N}_4$ carrier, because kaolinite is a 2D layered silicate composed of one tetrahedrally-coordinated sheet of silicon and one octahedrally-coordinated sheet of aluminum, which is similar to the 2D structure of $\text{g-C}_3\text{N}_4$ [26]. Therefore, a 2D/2D composite structure could be established by the combination of the kaolinite and $\text{g-C}_3\text{N}_4$ photocatalyst, which would significantly improve the photocatalytic efficiency of catalysts. For the past few years, our group has focused on the photocatalytic performance of $\text{g-C}_3\text{N}_4/\text{kaolinite}$ composite [26–28]. However, the photocatalytic performance, especially in visible light, is still limited. Hence, how to further improve the visible photocatalytic activity of $\text{g-C}_3\text{N}_4/\text{kaolinite}$ composite has become the key to the large-scale application of this material.

In our present study, we synthesize a novel kind of $\text{g-C}_3\text{N}_4/\text{kaolinite}$ composite through a two-step process using cyanuric acid as a modifier. The physicochemical properties of as-prepared composites were systematically analyzed. Furthermore, the photocatalytic performance of cyanuric-acid-modified $\text{g-C}_3\text{N}_4/\text{kaolinite}$ composites were evaluated by the photo-degradation of rhodamine B under visible-light irradiation. The influence of the cyanuric acid modifier amounts on visible-light photocatalytic efficiency of the as-prepared photocatalysts was probed. The possible mechanism of photocatalytic performance was also proposed and discussed. Our work is beneficial for better understanding the enhancement mechanism of mineral-based composite photocatalysts and designing more efficient metal-free, mineral-based photocatalytic composites for wastewater treatment.

2. Materials and Methods

2.1. Materials

The purified kaolinite (denoted as KA) was acquired from Suzhou City, China. Melamine ($C_3H_6N_6$) was bought from Jiaxing Sicheng Chemical Co., Ltd. (Zhejiang, China). Cyanuric acid ($C_3H_3N_3O_3$) and p-Benzoquinone (BQ) were purchased from Sinopharm Chemical Reagent Co. (Beijing, China). Beijing Reagent Co. (Beijing, China) provided rhodamine B ($C_{28}H_{31}C_1N_2O_3$, RhB), tert-butanol (TBA), edetate disodium (EDTA-2Na), and other chemicals used in our studies. The commercially available Degussa P25 was employed as reference. All of the chemicals were analytical reagent grade without further treatment and deionized water was used throughout this study.

2.2. Catalysts Preparation

The $g\text{-}C_3N_4$ (denoted as CN) sample was synthesized by thermal polymerization of melamine in air, which was based on our previous reports [29]. Twenty grams of melamine was added into an alumina crucible with a cover and heated to $550\text{ }^\circ\text{C}$ at a heating rate of $2.3\text{ }^\circ\text{C}\cdot\text{min}^{-1}$ and kept at this temperature for 4 h. After cooling down to room temperature, the sample was further heated to $500\text{ }^\circ\text{C}$ for 2 h in an open-air-atmosphere tube furnace with a heating rate of $5\text{ }^\circ\text{C}\cdot\text{min}^{-1}$. The final resultant yellow product was ground into powder for further use.

For synthesizing cyanuric-acid-modified $g\text{-}C_3N_4$ /kaolinite (denoted as m-CN/KA) composites, we followed a facile two-step procedure; wet impregnation and thermal polymerization processes. In detail, first, 4 g of melamine and various amounts of cyanuric acid were added into 50 mL of deionized water and stirred until the chemicals dissolved completely. Then, 2 g of purified kaolinite (KA) were dispersed into the above solution with uniform stirring for 12 h. After, the mixture was evaporated at $60\text{ }^\circ\text{C}$ using a water bath with continuous stirring. The resulting powder was calcined under the same conditions as those of the CN catalyst. Thermogravimetric analysis (TG) results showed that the content of graphitic carbon nitride in the CN/KA composite could be calculated as 38.82%, which was in accordance with the theoretical loading amount (40%). For comparison, $g\text{-}C_3N_4$ /kaolinite (denote as CN/KA) composites were also synthesized according to the above steps in the absence of the cyanuric acid modifier. The m-CN/KA samples with different cyanuric acid modifier amounts with respect to m-CN/KA were labeled as m-CN/KA-0.5, m-CN/KA-1, m-CN/KA-2, m-CN/KA-3, and m-CN/KA-4, respectively. The number at the end of each label corresponds to the additive mass of cyanuric acid.

2.3. Characterization

The phase properties of the as-prepared composites were detected using a D8 advance X-ray diffractometer (Bruker, Karlsruhe, Germany) with $\text{Cu-K}\alpha$ radiation ($\lambda = 0.154056\text{ nm}$), which were scanned in the range of 2θ from 10° to 80° with a 0.02° step at a scanning speed of $4^\circ\cdot\text{min}^{-1}$. The Brunauer-Emmett-Teller (BET) specific surface areas and pore size distributions of the as-prepared composites were determined by nitrogen adsorption instrument equipped with a JW-BK nitrogen adsorption apparatus (JWGB Sci. & Tech, Beijing, China) at 77 K . The morphology of the as-received composites was determined on an S-4800 scanning electron microscope (SEM) (Hitachi, Tokyo, Japan). Fourier transform infrared (FT-IR) spectroscopy was investigated using a ThermoFisher Nicolet 6700 spectrometer (Thermo Fisher Scientific, Waltham, MA, USA), which was prepared using potassium bromide (KBr) pellets. A METTLER SF/1382 thermal analyzer (Columbus, OH, USA) was employed to probe the thermogravimetric analysis (TG) under an O_2 atmosphere at a heating rate of $10\text{ }^\circ\text{C}\cdot\text{min}^{-1}$, from ambient temperature to $1000\text{ }^\circ\text{C}$. UV-vis diffuse reflectance spectrometry (UV-vis DRS) was also applied in this study, and the UV-vis absorption spectra were obtained using a UV-vis spectrophotometer (U-3100, Hitachi, Tokyo, Japan), where BaSO_4 was used as the reference.

2.4. Photoactivity Measurements

To evaluate the photocatalytic activities of the as-received catalysts, the photo-degradation performance of rhodamine B (RhB) aqueous solution was determined using a 500-W Xenon lamp with a 420-nm cut-off filter, which could guarantee the same wavelength as visible-light irradiation (BL-GHX-V, Shanghai Bilang plant, China). In a typical experiment, 0.2 g of the as-received composites were dispersed in 100 mL of RhB ($10 \text{ mg}\cdot\text{L}^{-1}$) aqueous solution by sonicating for 5 min in a quartz tube. To achieve the establishment of an adsorption/desorption equilibrium, 1 h of dark reaction was conducted before visible-light irradiation. At specific time intervals, 4 mL of suspension was collected and centrifuged, then the absorbance of the supernatant was measured at 554 nm using a UV-vis spectrophotometer, which reflected the photodegradation performance of the composites. Throughout the reaction, the catalyst was uniformly dispersed in the solution using a magnetic stirrer. The Degussa P25, CN and CN/KA composites served as references under the same conditions to carry out comparative experiments.

2.5. Computational Method

In this work, theoretical calculations were conducted in the CASTEP code using the Density Function Theory (DFT) approach. During the calculation, the Perdew-Burke-Ernzerhof (PBE) exchange-correlation function and spin-polarized generalized gradient approximation (GGA) exchange-correlation functions were used. The interaction effects between the layered mineral (i.e., kaolinite) and the g-C₃N₄ were described by the ultrasoft pseudopotential. The modification effect of cyanuric acid towards the g-C₃N₄/kaolinite system was also researched. During model construction, the structure of g-C₃N₄ was introduced into the primitive cell of kaolinite to construct the composites. The kinetic cut-off energy was set at 340 eV for the plane wave expansion, the threshold values were 0.001 Å for maximum displacement based on the convergence criteria, the maximum stress was 0.05 GPa, maximum force was 0.03 eV/Å, energy tolerance was 1.0×10^{-5} eV/atom, and self-consistent field tolerance was 1.0×10^{-6} eV/atom.

3. Results and Discussion

3.1. XRD Analyses

XRD patterns of CN, KA, CN/KA, and m-CN/KA composites with various cyanuric acid modifier amounts are shown in Figure 1. For kaolinite, the characteristic diffraction peaks at 12.43°, 20.00°, 25.01°, and 38.75° can be indexed as (001), (020), (002), and (200) diffraction planes, which are in line with the patterns of kaolinite (JCPDS No. 29-1490). It was found that the kaolinite characteristic diffraction peaks were not detected in the XRD patterns of CN/KA or m-CN/KA composites, which indicated that the kaolinite in composites were presumably becoming amorphous after calcination [26–28]. Additionally, the XRD pattern of CN exhibited a weak peak at 13.12° and an intense peak at 27.67°, consistent with the interlayer distance of 0.671 nm and 0.324 nm, which could be indexed as the (100) and (002) lattice planes of g-C₃N₄ (JCPDS No. 87-1526), respectively. The former peak was due to the S-triazine structural arrangement of inter-layer packing and the latter peak could be ascribed to the long-range interplanar stacking of conjugated aromatic systems of the g-C₃N₄ catalyst. From the XRD patterns of CN/KA and m-CN/KA composites, it was obvious that they displayed only one peak at 27.67° (002), which signified that g-C₃N₄ was successfully loaded onto the surface of kaolinite. As for the characteristic peak of g-C₃N₄ at 13.12° (100), it disappeared, as exhibited in the composites, owing to the low catalyst content and low intensity. Furthermore, there was no obvious difference among the XRD patterns of CN/KA and m-CN/KA composites. Hence, it can be inferred that the introduction of cyanuric acid has little significant influence on the crystallographic structure of g-C₃N₄ in composites.

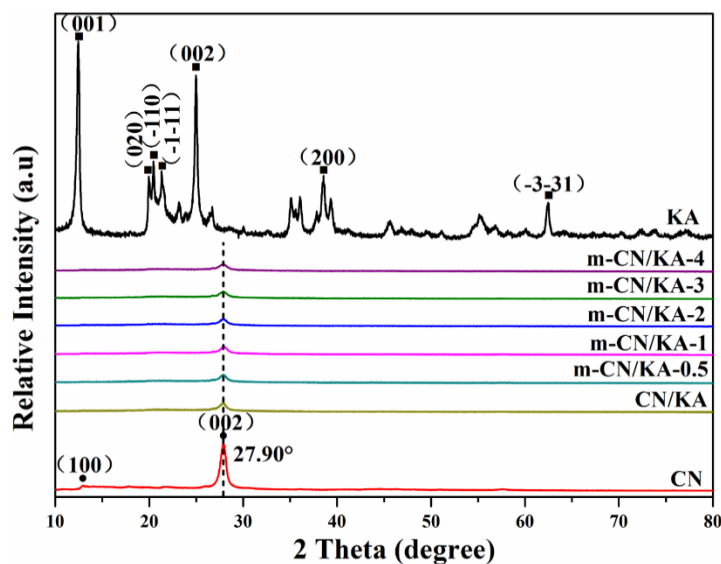


Figure 1. XRD patterns of KA, CN, CN/KA composite and m-CN/KA composites with various cyanuric acid modifier amounts.

3.2. Morphology Analysis

The morphology of CN, KA, CN/KA, and m-CN/KA-4 was identified using a scanning electron microscope (SEM), as observed in Figure 2. From Figure 2a, KA possesses a typical two-dimensional layered structure composed of many parallel nanosheets, which might, not only provide large surface area for enhancing adsorption ability, but also closely integrate with g-C₃N₄ nanosheets in the composites. Furthermore, the smooth and regular surface, without impurities, would also be significantly beneficial in the loading of g-C₃N₄. According to Figure 2b, a two-dimensional layered structure with bulk morphology was formed, owing to the aggregation effect, forming in the process of thermal polymerization. This would be the disadvantage to the contact between catalysts and pollution molecules in photocatalytic processes, and further decrease the migration of the photo-generated carrier, which results in a poor adsorption capacity and low quantum efficiency of pure g-C₃N₄. As illustrated in Figure 2c, the as-prepared CN/KA composite still maintained the original lamellar structure of kaolinite, but the lamellar surface became rougher and the edges became smoother. The morphology varieties showed that the g-C₃N₄ was successfully loaded onto the kaolinite surface and had an effective interfacial bond. Compared with CN, the introduction of KA promoted the dispersion of g-C₃N₄ in CN/KA composite, which would be favorable for the improvement of photoactivity. As shown in Figure 2d, compared with the CN/KA composite, the surface of g-C₃N₄/kaolinite became more porous and uniform after cyanuric acid modification, which should be responsible for the complete volatilization of cyanuric acid in precursor during the calcination process. In summary, the introduction of cyanuric acid effectively improved the pore structure of g-C₃N₄ in a binary system, providing more active sites for pollutant photodegradation.

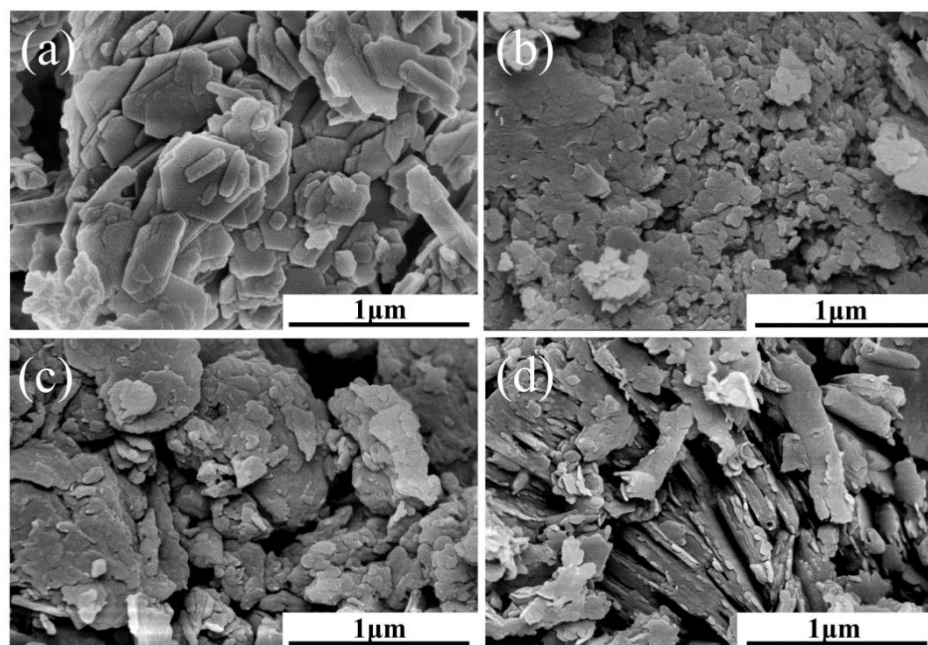


Figure 2. SEM images of (a) KA, (b) CN, (c) CN/KA composite, (d) m-CN/KA-4 composite.

3.3. BET Analysis

To further investigate the pore structure in CN, KA, CN/KA, and m-CN/KA-4 composites, the BET surface area, pore volume and average pore diameter (calculated by Barrett-Joyner-Halenda method) were examined by the N_2 adsorption-desorption isotherms, and the obtained results are listed in Table 1. According to Table 1, among the as-prepared samples, it is apparent that m-CN/KA-4 possesses the largest BET surface area and pore volume, which are almost twice those of CN. The larger surface area and total pore volume of the m-CN/KA composites could effectively enhance adsorption and photocatalytic ability, which account for the uniform distribution of $g\text{-C}_3\text{N}_4$ on kaolinite and the volatilization of cyanuric acid according to the previous morphological analysis results. As shown in Figure 3, the N_2 adsorption-desorption isotherms of CN/KA and m-CN/KA displayed a typical IV adsorption isotherm with a H3 hysteresis loop on the basis of the International Union of Pure and Applied Chemistry (IUPAC), which is the standard state of the mesoporous structure [30]. As for CN and KA, both showed a typical II adsorption isotherm, which was attributed to the nonporous and microporous structure. Furthermore, as shown in Figure 3b, after modification, the number of pores within 2 nm to 4 nm increased significantly, and a wider pore size distribution, from 1 nm to 20 nm, was obtained, which would also favor of the adsorption and photodegradation of a target pollutant.

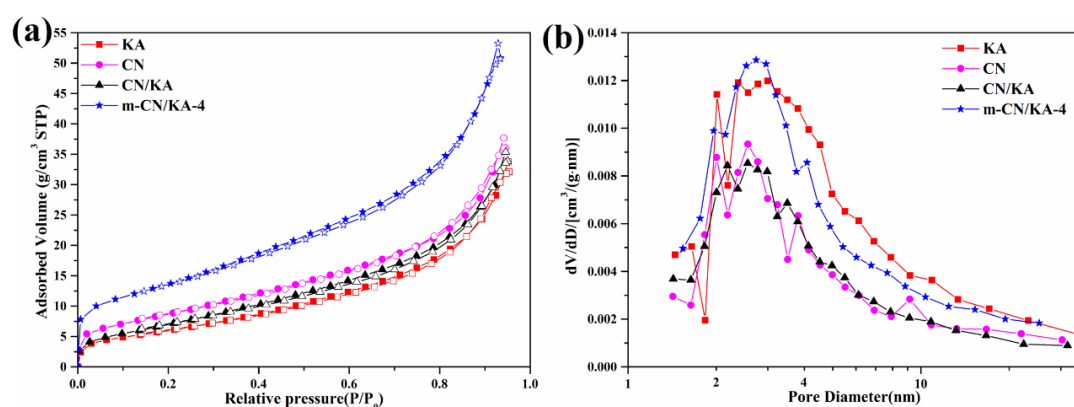


Figure 3. (a) N_2 adsorption isotherm and (b) pore-size distribution curves of CN, KA, CN/KA composite, and m-CN/KA-4 composite.

Table 1. BET surface area, pore volume, and average pore size of m-CN/KA composites with various modifier amounts.

Samples	Surface Area ($\text{m}^2 \cdot \text{g}^{-1}$)	Pore Volume ($\text{cm}^3 \cdot \text{g}^{-1}$)	Average Pore Size (nm)
KA	22.957	0.059	6.979
CN	29.672	0.066	7.100
CN/KA	27.378	0.062	6.610
m-CN/KA-0.5	28.562	0.063	6.591
m-CN/KA-1	33.835	0.066	6.445
m-CN/KA-2	40.632	0.076	6.434
m-CN/KA-3	44.519	0.082	6.309
m-CN/KA-4	49.522	0.088	6.251

3.4. Optical Properties

A UV-vis diffuse reflection spectrum (DRS) was applied to inspect the optical absorption properties of KA, CN, CN/KA, and m-CN/KA composites. As illustrated in Figure 4a, it is implied that all these as-prepared catalysts exhibited superior absorption capacity from the UV to visible light region. KA absorbed light from the UV to the visible region, while the bare CN started from around 480 nm. Moreover, it is obvious that the optical absorption of the as-prepared CN/KA and m-CN/KA composites was greatly enhanced within the scope of both UV and visible light compared with those of CN and KA, which can be attributed to the defects and vibration produced by intimate interfacial combination between g-C₃N₄ and kaolinite. Therefore, due to the stronger light absorption ability and the larger range of wavelengths and the photon absorption of as-prepared catalysts, more photogenerated electron-hole pairs would be created under irradiation, which might be a key factor to increase photodegradation efficiency. In addition, the band gaps of the as-prepared catalysts were calculated and are shown in Figure 4c,d. The calculated band gap of CN was 2.72 eV, and all the band gaps of the m-CN/KA composites were around 2.72 ± 0.01 eV, indicating that the introduction of cyanuric acid had little or no effect on the band gaps of g-C₃N₄.

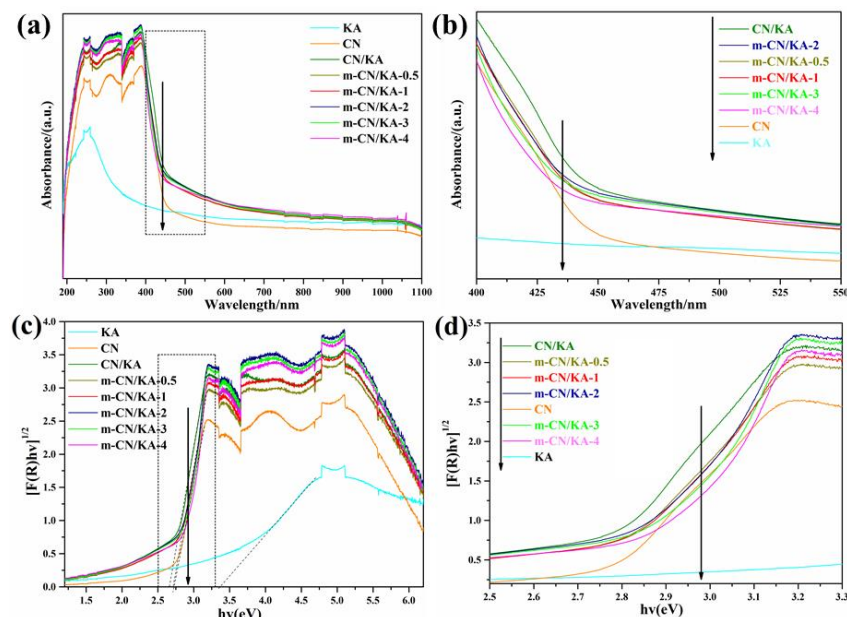


Figure 4. (a,b) UV-vis DRS and (c,d) band gaps of CN, KA, CN/KA composite, and m-CN/KA composites with different cyanuric acid modifier amounts.

3.5. FT-IR Analysis

The functional groups of KA, CN, CN/KA, and m-CN/KA-4 were analyzed using FT-IR spectroscopy, and the results are shown in Figure 5. Regarding KA, the strong peak at 3689 cm^{-1} and 3621 cm^{-1} denoted the OH stretching of inner surface hydroxyl and OH stretching of inner hydroxyl, respectively. The band in the range of around 1600 cm^{-1} to 1700 cm^{-1} represented the presence of co-intercalated water molecules. The peaks located in the range of 1100 cm^{-1} to 1000 cm^{-1} were assigned to the Si–O stretching. The band at 917 cm^{-1} displayed the Al–OH bending vibrations, and the bands at 787 cm^{-1} and 695 cm^{-1} were attributed to O–Al–OH absorption vibrations. The bands at 757 cm^{-1} and 540 cm^{-1} were related to the Al–O–Si deformations, and the bands at 465 cm^{-1} and 434 cm^{-1} referred to the Si–O–Si deformations. The characteristic infrared absorption bands between CN/KA and m-CN/KA-4 were similar, but the intensity of infrared absorption bands of m-CN/KA-4 was obviously weaker than that of CN/KA. The strong peak between 3000 and 3300 cm^{-1} corresponded to stretching of terminal NH_2 or NH groups caused by incomplete polycondensation of g-C₃N₄ at the defect sites of the aromatic ring. Compared with CN/KA, the intensity of absorption peaks corresponding to stretching of terminal NH_2 or NH groups obviously decreased, indicating that the addition of cyanuric acid promoted the polycondensation of g-C₃N₄ in the as-prepared composites, which significantly reduced the terminal NH_2 or NH groups. The absorption bands in the range of 1100 – 800 cm^{-1} corresponded to the Si–O stretching vibration and Al–OH bending vibration in kaolinite, where m-CN-KA-4 is significantly smoother. Hence, it shows that the reactive sites on the kaolinite surface decreased significantly, and the others were combined with g-C₃N₄ more effectively. It could be demonstrated that the g-C₃N₄ nanosheets had been attached to the layered kaolinite successfully and the distribution of g-C₃N₄ on the surface carrier became more uniform due to the introduction of cyanuric acid. In addition, there were no newborn functional groups in the m-CN-KA-4, indicating that the introduction of cyanuric acid did not change the functional groups of g-C₃N₄ in the as-prepared composites.

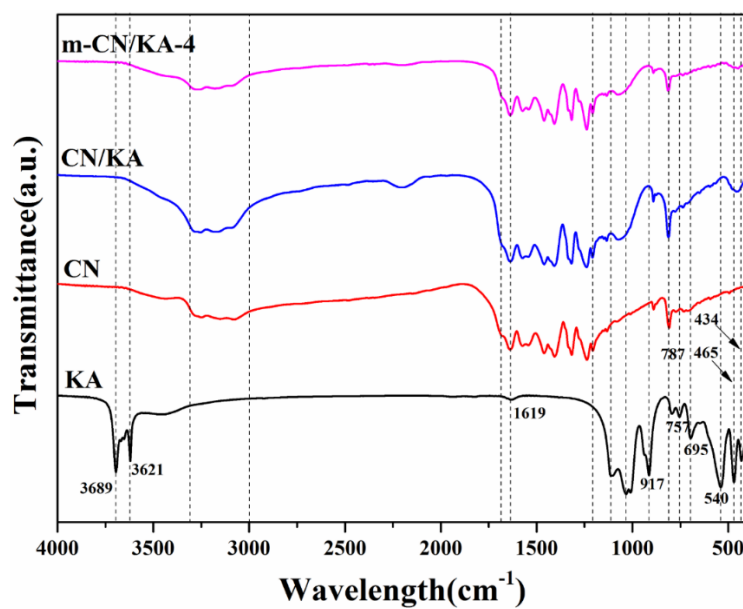


Figure 5. FT-IR spectra of CN, KA, CN/KA composite, and m-CN/KA-4 composite.

3.6. DFT Analysis

CASTEP, i.e., the Cambridge Sequential Total Energy Package, is a frequently-used module based on density functional theory (DFT). Through accessing the CASTEP module embedded within the material studio software (Materials Studio 8.0, Accelrys, San Diego, CA, USA), we can realize electronic structure calculations in many fields, including surfaces, molecules, solids, liquids, and amorphous

materials according to the first-principles calculations. In order to identify the interaction properties between g-C₃N₄ and kaolinite, as well as the function of cyanuric acid towards g-C₃N₄/kaolinite composite, we constructed a crystal model and calculated the band structure and density of states based on DFT calculations. Figure 6 presents the crystal structures of CN, KA, CN/KA, and m-CN/KA. The unit cell of kaolinite ($\alpha = 91.93^\circ$, $\beta = 105.04^\circ$, $\gamma = 89.79^\circ$, $a = 5.149 \text{ \AA}$, $b = 8.934 \text{ \AA}$, $c = 7.384 \text{ \AA}$) investigated in this research is also in line with previously reported results [31]. All the structures of the samples were constructed and exhibited based on a (010) surface. Based on a previous report, it is indicated that the cyanuric acid modified g-C₃N₄/kaolinite will make the substitution from nitrogen atom to carbon atom, as shown in Figure 6d [32].

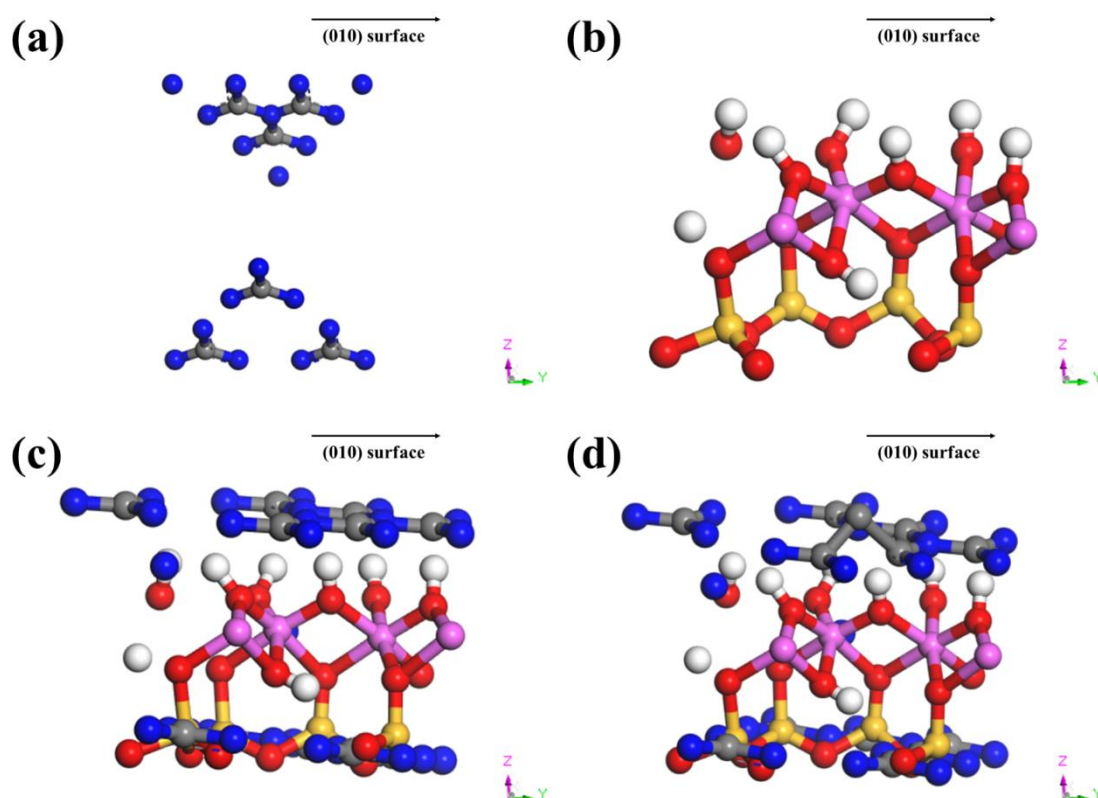


Figure 6. Side view of the basal (010) surfaces of (a) CN (C_6N_{21}), (b) KA ($H_8Si_4Al_4O_{18}$), (c) CN/KA ($2C_6N_{15}-H_8Si_4Al_4O_{18}$), and (d) m-CN/KA ($2C_7N_{14}-H_8Si_4Al_4O_{18}$). Color scheme (used for all figures): hydrogen, white; oxygen, red; aluminum, pink; silicon, yellow; carbon, gray; nitrogen, blue.

To further elucidate the enhanced photocatalytic performance of cyanuric-acid-modified g-C₃N₄/kaolinite, the band structure and density of states of CN, KA, CN/KA, and m-CN/KA were calculated using the Generalized Gradient Approximation/Perdew-Burke-Ernzerhof (GGA/PBE) method. As seen from Figure 7, bare g-C₃N₄ has a narrow band gap (0.896 eV) while bare kaolinite has a wide band gap (4.502 eV), demonstrating the semiconductor property and insulation property, respectively. After combination, the calculated band gaps of CN/KA and m-CN/KA were obviously decreased, which might contribute to the photogenerated carriers' excitation and migration. Nevertheless, the calculated band gaps were much lower than the experimental results, which should be ascribed to the well-known limitations of DFT. As for CN/KA and m-CN/KA, the electron orbital density was increased greatly in conduction band minimum (CBM), especially for m-CN/KA, indicating an improvement in the transfer efficiency of carriers and the reaction rate. Density of states were also taken to research the effect of cyanuric acid on g-C₃N₄/kaolinite composite. The results showed that the orbit was primarily located on the valance band and mainly composed of s and p orbitals for the single kaolinite. For the bare g-C₃N₄, the CB of g-C₃N₄ was mostly composed

by s and p orbitals. As for CN/KA and m-CN/KA, consecutive orbitals were mainly distributed in the range of -25 to 2.5 eV. It is indicated that the introduction of cyanuric acid caused the change in orbital constitutions. The increase of s and p orbital intensity in valence band maximum (VBM) could promote the augmentation of band density and be conducive to the improvement of quantum efficiency [31].

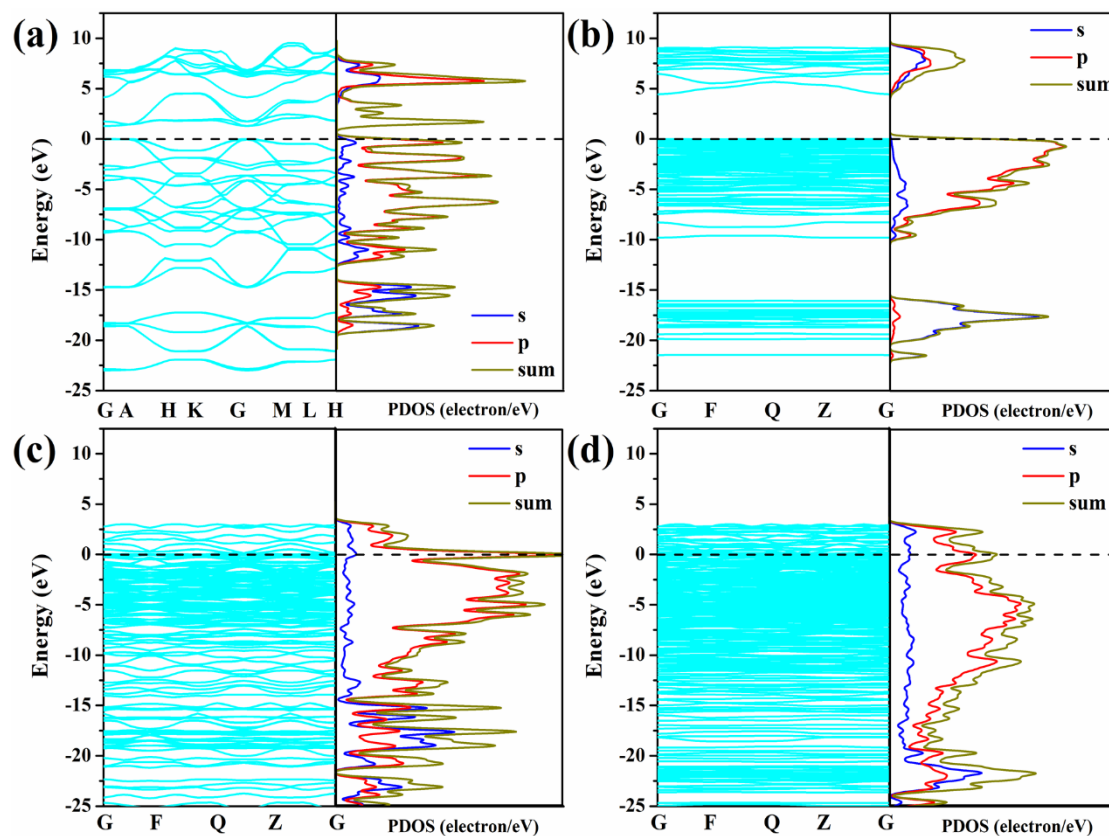


Figure 7. Band structures and partial density of states (PDOS) for (a) CN (C_6N_{21}), (b) KA ($H_8Si_4Al_4O_{18}$), (c) CN/KA ($2C_6N_{15}-H_8Si_4Al_4O_{18}$), and (d) m-CN/KA ($2C_7N_{14}-H_8Si_4Al_4O_{18}$).

3.7. Photocatalytic Performance

To specify the effect of cyanuric acid concentration on adsorption and photocatalytic performance, the photodegradation of RhB (10 mg/L) under visible light illumination was carried out for m-CN/KA composites using P25, CN, KA, and CN/KA as reference samples under the same conditions. All of the results are presented in average values \pm standard deviation of three replicates. As shown in Figure 8a, the RhB degradation ratio curves were calculated by C/C_0 of the as-prepared catalyst, where C_0 is the initial concentration of RhB and C is the concentration of RhB at time t . Clearly, all samples achieved equilibrium of adsorption and desorption between solution and catalysts in 60 min under dark condition prior to irradiation. Among all the as-prepared catalysts, the adsorption ability of CN was the lowest. On the other hand, the adsorption ability of m-CN/KA composites were gradually enhanced with increasing cyanuric acid amounts. All the as-prepared m-CN/KA composites had higher adsorption abilities compared with other samples, except KA. Under visible light illumination, KA showed no photoactivity towards RhB, while single CN had certain visible light photocatalytic activity. The CN/KA composite showed a higher photocatalytic performance than CN, because the graphite carbon nitride in the composite was uniformly distributed on the surface of the carrier kaolinite, solving the problem of low quantum efficiency caused by the thermal agglomeration process [31]. Furthermore, the introduction of kaolinite as the supporter of g-C₃N₄ provided more surface defects for the composites and improved the separation efficiency of photogenerated electron-hole pairs.

The addition of cyanuric acid could also effectively improve the adsorption ability of the composites. The improvement should be ascribed to the fact that cyanuric acid is decomposed at around 330 °C during the thermal polymerization process. As a result, a large number of pore structures and reactive sites were generated in the composites, greatly increasing the specific surface area of the composites, improving the adsorption ability and further enhancing the photocatalytic performance. The removal rate of RhB after 180 min of visible light illumination for m-CN/KA-4 was up to 93%, which was around two and nine times higher than bare g-C₃N₄ and standard P25, respectively.

To further quantitatively evaluate the photocatalytic performance of the m-CN/KA composites, the relative concentrations of RhB were fitted using the apparent pseudo-first-order rate equation, $\ln(C_0/C) = kt$, where C and C₀ were explained above and k is the apparent reaction rate constant. The results are listed in Table 2 and the curves are displayed in Figure 8b. From Table 2, it is obvious that the photo-degradation kinetics of RhB in the as-received catalysts showed significant linear relationships. In addition, with increasing cyanuric acid modifier amounts, the reaction constant rate of m-CN/KA composites exhibited an obvious increasing trend. The reaction constant rate of m-CN/KA-4 was over four times and seven times as much as that of bare g-C₃N₄ and standard P25, respectively.

Table 2. Parameters of the pseudo-first order for RhB degradation under visible light over P25, CN, KA, CN/KA, and m-CN/KA composites with various modifier amounts.

Sample	k (min ⁻¹)	Correlation Coefficient (R ²)
P25	0.0012	0.99
CN	0.0021	0.99
KA	2.502 × 10 ⁻⁴	0.87
CN/KA	0.0043	0.99
m-CN/KA-0.5	0.0048	0.99
m-CN/KA-1	0.0059	0.99
m-CN/KA-2	0.0064	0.97
m-CN/KA-3	0.0074	0.98
m-CN/KA-4	0.0086	0.98

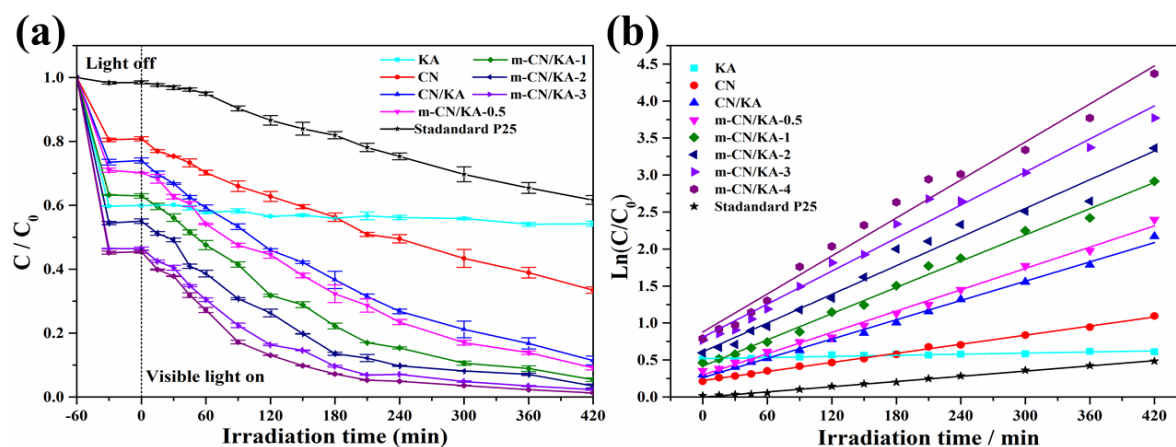


Figure 8. (a) Photodegradation of RhB by P25, CN, KA, CN/KA composite, and m-CN/KA composites with the average values \pm the standard deviation of three replicates under visible light and (b) the corresponding first-order kinetics plots.

3.8. Possible Mechanism

As is known, the three main active species in the photocatalytic process are photo-generated holes, ·OH radicals, and ·O₂⁻ radicals. Hence, in order to determine the crucial active species in the photodegradation process of as-prepared m-CN/KA-4 catalyst under visible light illumination, we

carried out a battery of radicals trapping experiments by employing edentate disodium (EDTA-2Na), 1,4-benzoquinone (BQ), and tert-Butanol (TBA) as scavengers for photo-generated holes (h^+), hydroxyl radicals ($\cdot\text{OH}$), and superoxide radicals ($\cdot\text{O}_2^-$), respectively. The dosage of all scavengers was 5 mM and the results are displayed in Figure 9. In absence of adding scavengers, it is obvious that the photocatalytic rate in degrading of RhB aqueous solution was up to almost 80% after 180 min of visible-light illumination. The addition of TBA exhibited a negligible influence on the RhB degradation of m-CN/KA-4 composite, revealing that the $\cdot\text{OH}$ radicals are not main radical species in the photocatalytic reaction system. On the other hand, the addition of EDTA-2Na had a significant influence on the photodegradation process under visible light, which indicates that the photo-generated holes (h^+) should be the most vital active species in the photodegradation process of the as-received m-CN/KA composites.

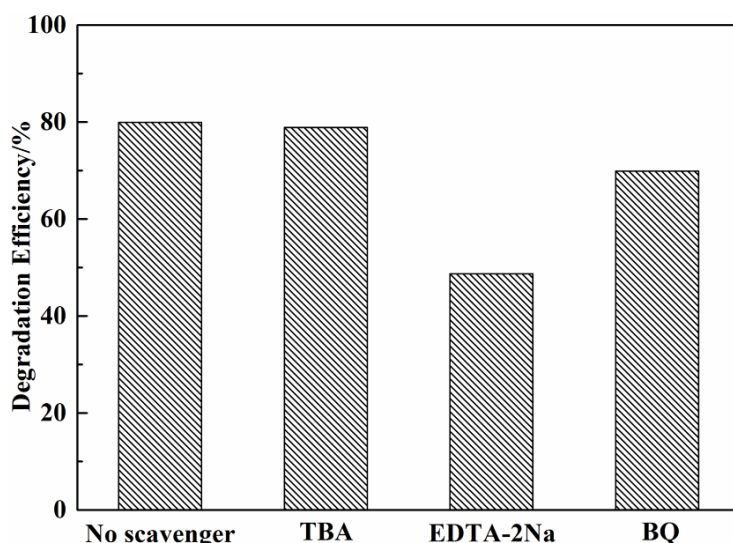
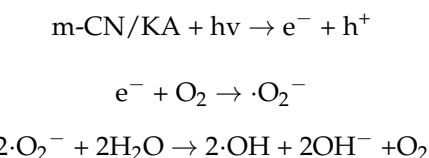


Figure 9. Trapping experimental results of active species for the photocatalytic degradation of RhB by m-CN/KA-4 composite under 180 min visible light illumination.

According to the above experimental results and previous literature reports [26,28], the main reactions could be inferred as follows:



The possible RhB degradation mechanism and potential electrons transfer pathway over m-CN/KA composites are described in Figure 10. Under visible-light irradiation, the electrons (e^-) of the valence band (VB) over the m-CN/KA composites excited to the conduction band (CB), forming holes (h^+) in the VB, which could directly oxidize RhB. As we all know, electrostatic repulsion exists between negatively-charged electrons, and electrostatic attraction exists between negatively charged electrons and positively charged electrons. For kaolinite, its layered surface is generally negatively charged [26–28,30]; therefore, the excited e^- on VB should be accelerated to migrate to CB and the e^- on the CB could be combined with the oxygen absorbed on the surface of the composite to produce superoxide ($\cdot\text{O}_2^-$). Then, the $\cdot\text{O}_2^-$ would react with water molecules to produce hydroxyl radicals ($\cdot\text{OH}$), OH^- and O_2 , and the product $\cdot\text{OH}$ could also react with RhB. Furthermore, electrostatic attraction between the negatively-charged kaolinite layers and RhB in the solution can also make an enhancement on the photocatalytic performance of m-CN/KA composite.

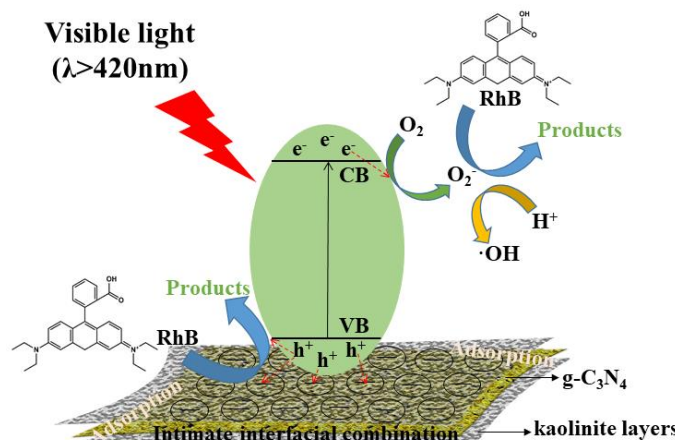


Figure 10. Schematic illustration of the charge separation and photocatalytic mechanism of m-CN/KA composites under visible light irradiation.

4. Conclusions

In summary, a novel kind of cyanuric-acid-modified $\text{g-C}_3\text{N}_4$ /kaolinite (m-CN/KA) composite with enhanced visible light photocatalytic activity was prepared through a facile two-step method in this study. The as-received cyanuric-acid-modified $\text{g-C}_3\text{N}_4$ /kaolinite composite possesses enhanced photocatalytic performance in RhB degradation under visible-light irradiation, the apparent rate constant of which was almost two times that of the $\text{g-C}_3\text{N}_4$ /kaolinite and over four times that of bare $\text{g-C}_3\text{N}_4$. Based on the characterization results and DFT analyses, the improvement of the photocatalytic performance should be ascribed, not only to the generation of abundant pore structures and reactive sites, but also to the efficient separation of the photogenerated electron-hole pairs because of the intimate interfacial combination of $\text{g-C}_3\text{N}_4$ and kaolinite. Combined with the characterization results and the radical scavenger experiments, it is indicated that the formed intimate interfacial combination between $\text{g-C}_3\text{N}_4$ and kaolinite could reduce the combination of the photogenerated electron-hole pairs efficiently, which improves the utilization efficiency of a photo-generated carrier, thus enhancing the photocatalytic activity of composites. Our present study can provide new insight into the preparation of visible light-driven composite photocatalysts based on natural minerals, which exhibit potential industrial applications in the field of organic dye degradation.

Author Contributions: Conceptualization, Z.S. and B.W.; data curation, Z.S. and F.Y.; investigation, F.Y., X.L. and J.X.; project administration, Z.S.; software, C.L.; supervision, Z.S.; writing—original draft, Z.S. and F.Y.; writing—review and editing, Z.S. and B.W.

Funding: This research was funded by the National Key R&D Program of China (2017YFB0310803-4), the Young Elite Scientists Sponsorship Program by CAST (2017QNRC001), the Yueqi Funding Scheme for Young Scholars (China University of Mining & Technology, Beijing), the Beijing Excellent Talent Training Subsidy Program—Youth Backbone (2017000020124G089), and the Youth Backbone Teacher Growth Support Plan of Beijing Institute of Fashion Technology (BIFTQG201807).

Conflicts of Interest: The authors declare no conflicts of interest.

References

- Chi, C.; Chen, W.; Guo, M.; Weng, M.; Yan, G.; Shen, X. Law and features of TVOC and Formaldehyde pollution in urban indoor air. *Atmos. Environ.* **2016**, *132*, 85–90. [[CrossRef](#)]
- Sun, Y.; Wang, P.; Zhang, Q.; Ma, H.; Hou, J.; Kong, X. Indoor Air Pollution and Human Perception in Public Buildings in Tianjin, China. *Procedia Eng.* **2015**, *121*, 552–557. [[CrossRef](#)]
- Luengas, A.; Barona, A.; Hort, C.; Gallastegui, G.; Platel, V.; Elias, A. A review of indoor air treatment technologies. *Rev. Environ. Sci. Bio/Technol.* **2015**, *14*, 499–522. [[CrossRef](#)]
- Kurniawan, T.A.; Chan, G.Y.S.; Lo, W.; Babel, S. Physico-chemical treatment techniques for wastewater laden with heavy metals. *Chem. Eng. J.* **2006**, *118*, 83–98. [[CrossRef](#)]

5. Wang, S.; Peng, Y. Natural zeolites as effective adsorbents in water and wastewater treatment. *Chem. Eng. J.* **2010**, *156*, 11–24. [[CrossRef](#)]
6. Zhao, Y.; Huang, J.; Zhao, H.; Yang, H. Microbial community and N removal of aerobic granular sludge at high COD and N loading rates. *Bioresour. Technol.* **2013**, *143*, 439–446. [[CrossRef](#)] [[PubMed](#)]
7. Maeda, K.; Takata, T.; Hara, M.; Saito, N.; Inoue, Y.; Kobayashi, H.; Domen, K. GaN:ZnO Solid Solution as a Photocatalyst for Visible-Light-Driven Overall Water Splitting. *J. Am. Chem. Soc.* **2005**, *127*, 8286–8287. [[CrossRef](#)] [[PubMed](#)]
8. Ni, M.; Leung, M.K.H.; Leung, D.Y.C.; Sumathy, K. A review and recent developments in photocatalytic water-splitting using TiO₂ for hydrogen production. *Renew. Sustain. Energy Rev.* **2007**, *11*, 401–425. [[CrossRef](#)]
9. Jayamohan, H.; Smith, Y.R.; Hansen, L.C.; Mohanty, S.K.; Gale, B.K.; Misra, M. Anodized titania nanotube array microfluidic device for photocatalytic application: Experiment and simulation. *Appl. Catal. B Environ.* **2015**, *174–175*, 167–175. [[CrossRef](#)]
10. Dong, H.; Guo, X.; Yang, C.; Ouyang, Z. Synthesis of g-C₃N₄ by different precursors under burning explosion effect and its photocatalytic degradation for tylosin. *Appl. Catal. B Environ.* **2018**, *230*, 65–76. [[CrossRef](#)]
11. Wang, X.; Maeda, K.; Thomas, A.; Takanabe, K.; Xin, G.; Carlsson, J.M.; Domen, K.; Antonietti, M. A metal-free polymeric photocatalyst for hydrogen production from water under visible light. *Nat. Mater.* **2008**, *8*, 76. [[CrossRef](#)] [[PubMed](#)]
12. Niu, P.; Zhang, L.; Liu, G.; Cheng, H. Graphene-Like Carbon Nitride Nanosheets for Improved Photocatalytic Activities. *Adv. Funct. Mater.* **2012**, *22*, 4763–4770. [[CrossRef](#)]
13. Fang, L.; Ohfuji, H.; Shinmei, T.; Irihara, T. Experimental study on the stability of graphitic C₃N₄ under high pressure and high temperature. *Diam. Relat. Mater.* **2011**, *20*, 819–825. [[CrossRef](#)]
14. Wang, M.; Cui, S.; Yang, X.; Bi, W. Synthesis of g-C₃N₄/Fe₃O₄ nanocomposites and application as a new sorbent for solid phase extraction of polycyclic aromatic hydrocarbons in water samples. *Talanta* **2015**, *132*, 922–928. [[CrossRef](#)] [[PubMed](#)]
15. Kundoo, S.; Banerjee, A.N.; Saha, P.; Chattopadhyay, K.K. Synthesis of crystalline carbon nitride thin films by electrolysis of methanol–urea solution. *Mater. Lett.* **2003**, *57*, 2193–2197. [[CrossRef](#)]
16. Yan, S.C.; Li, Z.S.; Zou, Z.G. Photodegradation Performance of g-C₃N₄ Fabricated by Directly Heating Melamine. *Langmuir* **2009**, *25*, 10397–10401. [[CrossRef](#)] [[PubMed](#)]
17. Sano, T.; Tsutsui, S.; Koike, K.; Hirakawa, T.; Teramoto, Y.; Negishi, N.; Takeuchi, K. Activation of graphitic carbon nitride (g-C₃N₄) by alkaline hydrothermal treatment for photocatalytic NO oxidation in gas phase. *J. Mater. Chem. A* **2013**, *1*, 6489. [[CrossRef](#)]
18. Wang, Y.; Zhao, S.; Zhang, Y.; Fang, J.; Zhou, Y.; Yuan, S.; Zhang, C.; Chen, W. One-pot synthesis of K-doped g-C₃N₄ nanosheets with enhanced photocatalytic hydrogen production under visible-light irradiation. *Appl. Surf. Sci.* **2018**, *440*, 258–265. [[CrossRef](#)]
19. Sridharan, K.; Jang, E.; Park, T.J. Novel visible light active graphitic C₃N₄–TiO₂ composite photocatalyst: Synergistic synthesis, growth and photocatalytic treatment of hazardous pollutants. *Appl. Catal. B Environ.* **2013**, *142–143*, 718–728. [[CrossRef](#)]
20. Shalom, M.; Inal, S.; Fettkenhauer, C.; Neher, D.; Antonietti, M. Improving Carbon Nitride Photocatalysis by Supramolecular Preorganization of Monomers. *J. Am. Chem. Soc.* **2013**, *135*, 7118–7121. [[CrossRef](#)] [[PubMed](#)]
21. Perera, S.D.; Mariano, R.G.; Vu, K.; Nour, N.; Seitz, O.; Chabal, Y.; Balkus, K.J. Hydrothermal Synthesis of Graphene-TiO₂ Nanotube Composites with Enhanced Photocatalytic Activity. *ACS Catal.* **2012**, *2*, 949–956. [[CrossRef](#)]
22. Wang, B.; Zhang, G.; Leng, X.; Sun, Z.; Zheng, S. Characterization and improved solar light activity of vanadium doped TiO₂/diatomite hybrid catalysts. *J. Hazard. Mater.* **2015**, *285*, 212–220. [[CrossRef](#)] [[PubMed](#)]
23. Sun, Z.; Zhang, Y.; Zheng, S.; Park, Y.; Frost, R.L. Preparation and thermal energy storage properties of paraffin/calcined diatomite composites as form-stable phase change materials. *Thermochim. Acta* **2013**, *558*, 16–21. [[CrossRef](#)]
24. Zhang, G.; Sun, Z.; Duan, Y.; Ma, R.; Zheng, S. Synthesis of nano-TiO₂/diatomite composite and its photocatalytic degradation of gaseous formaldehyde. *Appl. Surf. Sci.* **2017**, *412*, 105–112. [[CrossRef](#)]
25. Li, C.; Sun, Z.; Huang, W.; Zheng, S. Facile synthesis of g-C₃N₄/montmorillonite composite with enhanced visible light photodegradation of rhodamine B and tetracycline. *J. Taiwan Inst. Chem. Eng.* **2016**, *66*, 363–371. [[CrossRef](#)]

26. Sun, Z.; Yao, G.; Zhang, X.; Zheng, S.; Frost, R.L. Enhanced visible-light photocatalytic activity of kaolinite/g-C₃N₄ composite synthesized via mechanochemical treatment. *Appl. Clay Sci.* **2016**, *129*, 7–14. [[CrossRef](#)]
27. Li, C.; Sun, Z.; Zhang, W.; Yu, C.; Zheng, S. Highly efficient g-C₃N₄/TiO₂ /kaolinite composite with novel three-dimensional structure and enhanced visible light responding ability towards ciprofloxacin and *S. aureus*. *Appl. Catal. B Environ.* **2018**, *220*, 272–282. [[CrossRef](#)]
28. Dong, X.; Sun, Z.; Zhang, X.; Li, C.; Zheng, S. Construction of BiOCl/g-C₃N₄ /kaolinite composite and its enhanced photocatalysis performance under visible-light irradiation. *J. Taiwan Inst. Chem. Eng.* **2018**, *84*, 203–211. [[CrossRef](#)]
29. Li, C.; Sun, Z.; Li, X.; Liu, L.; Zheng, S. Facile fabrication of g-C₃N₄/precipitated silica composite with enhanced visible-light photoactivity for the degradation of rhodamine B and Congo red. *Adv. Power Technol.* **2016**, *27*, 2051–2060. [[CrossRef](#)]
30. Thommes, M.; Kaneko, K.; Neimark, A.V.; Olivier, J.P.; Rodriguez-Reinoso, F.; Rouquerol, J.; Sing, K.S.W. Physisorption of gases, with special reference to the evaluation of surface area and pore size distribution (IUPAC Technical Report). *Pure Appl. Chem.* **2015**, *87*, 1051–1069. [[CrossRef](#)]
31. Sun, Z.; Li, C.; Du, X.; Zheng, S.; Wang, G. Facile synthesis of two clay minerals supported graphitic carbon nitride composites as highly efficient visible-light-driven photocatalysts. *J. Colloid Interface Sci.* **2018**, *511*, 268–276. [[CrossRef](#)] [[PubMed](#)]
32. Zheng, Q.; Durkin, D.P.; Elenewski, J.E.; Sun, Y.; Banek, N.A.; Hua, L.; Chen, H.; Wagner, M.J.; Zhang, W.; Shuai, D. Visible-light-responsive graphitic carbon nitride: Rational design and photocatalytic applications for water treatment. *Environ. Sci. Technol.* **2016**, *50*, 12938–12948. [[CrossRef](#)] [[PubMed](#)]



© 2018 by the authors. Licensee MDPI, Basel, Switzerland. This article is an open access article distributed under the terms and conditions of the Creative Commons Attribution (CC BY) license (<http://creativecommons.org/licenses/by/4.0/>).